aer

Atmospheric and
Environmental Research, Inc.

Final Report for SENH99-0000-0125

Real Time Monitoring of Flooding From Microwave Satellite Observations

Performance period: 1 October 2000 — 30 September 2002

6 September 2002

Contract No. NAS5-00189

By: John F. Galantowicz (PI)

Prepared by:
Atmospheric and Environmental Research, Inc.
131 Hartwell Ave.
Lexington, MA 02421

Prepared for:
Dr. Herb Frey (COTR)
Geodynamics Branch
NASA Goddard Space Flight Center
Code 921
Greenbelt, MD 20771

AER Document: P870-FR-I-20020906

This page intentionally left blank.

TABLE OF CONTENTS

LIST OF FIGURES

This page intentionally left blank.

ABSTRACT

We have developed a new method for making high-resolution flood extent maps (e.g., at the 30-100 m scale of digital elevation models) in real-time from low-resolution (20-70 km) passive microwave observations. The method builds a "flood-potential" database from elevations and historic flood imagery and uses it to create a flood-extent map consistent with the observed open water fraction. Microwave radiometric measurements are useful for flood monitoring because they sense surface water in clear-or-cloudy conditions and can provide more timely data (e.g., compared to radars) from relatively wide swath widths and an increasing number of available platforms (DMSP, ADEOS-II, Terra, NPOESS, GPM). The chief disadvantages for flood mapping are the radiometers' low resolution and the need for local calibration of the relationship between radiances and open-water fraction. We present our method for transforming microwave sensor-scale open water fraction estimates into high-resolution flood extent maps and describe 30-day flood map sequences generated during a retrospective study of the 1993 Great Midwest Flood. We discuss the method's potential improvement through as yet unimplemented algorithm enhancements and expected advancements in microwave radiometry (e.g., improved resolution and atmospheric correction).

1. Introduction

Open water has a very different microwave spectral signature than land surfaces and flooded areas are easily seen in microwave imagery. For example, NOAA routinely produces a global experimental wetness index based on low-resolution 19 and 85 GHz SSM/I channels. (http://orbit-net.nesdis.noaa.gov/arad/ht/ff/index3.html). Microwave sensors (SSM/I, TMI, AMSR, SSMIS, CMIS) are well suited for this task because they can see through cloud cover and cloud cover is expected to be persistent through many large-scale flood events. However microwave sensor resolutions are typically 25-70 km and useful maps of even the largest floods should have 1 km resolution or better. Our flood mapping method retrieves the fractional area of open water in real-time from low-resolution passive microwave data and makes high-resolution flood maps by merging the retrieved open water fraction with a flood-potential database. The flood-potential database is built a priori from high-resolution (<100 m) digital elevation models (DEM), land-use maps, and historic flood extent maps.

Passive microwave data have already been used to observe inundated areas. For instance, [1], [2], and [3] used the 37 GHz polarization difference signal of SMMR to detect the inundation patterns in the Amazon River basin. They showed that the flood-extent signal was strong in the microwave data despite the heavy canopy cover found throughout the surrounding flood plain.

Passive microwave sensors are preferable over other observing systems for monitoring flooding because they provide frequent observations relatively unaffected by cloudiness. Furthermore, planned sensors such as SSMIS (to be launched 10/2002) and CMIS (2009) and the proposed Global Precipitation Mission (GPM) will further improve refresh rates, atmospheric and surface temperature correction, and/or spatial resolution.

Our method is designed to ameliorate the main defect of the SSM/I-like sensors—namely their relatively large footprint size—through integration with high-resolution datasets. During developing flood events, the technique can provide real-time estimates of inundation extent to help emergency management personal allocate limited resources. Also, time-evolving, detailed maps of past flood events can aid studies in the fields of hydrology, meteorology, agriculture, ecology, insurance, and land management. The method can both augment flood monitoring in data-rich areas—e.g., by providing spatial context for stream gauge and other point

observations—as well as fill the temporal gap left when cloud-sensitive remote sensing techniques are the main quantitative flood monitoring method, such as in lesser-developed countries.

2. Flood mapping procedure

The flood mapping procedure consists of three main steps: Derivation of a "flood-potential" database, calibration of the microwave flood-fraction algorithm, and production of the high-resolution flood map itself. The first two steps are carried out off-line for each region of interest (about the size of a sensor field-of-view, or FOV) with flood-potential derivation being by far the most computationally intensive step. The final step can be performed quickly as microwave data become available. We describe each step below with additional details provided in the Appendix.

2.1. Derivation of the flood-potential database

Figure 2-1 shows four maps that summarize the development of a flood-potential database; each step is described below and with additional detail in appendix G. The dashed circle is the nominal 70 km SSM/I 3dB FOV corresponding to an EASE-Grid grid point [4]. (The true FOVs are randomly oriented ellipses approximately 70x43 km.) Each map is overlaid with the maximum-extent limits of the 1993 Midwest Flood derived by SAST (Scientific Assessment and Strategy Team, http://edcwww2.cr.usgs.gov/sast-home.html) from multiple clear-sky Landsat and SPOT and some radar images (see appendix A). Land-use open water maps (shown upper left, see appendix C) and the maximum flood extent map constrain the microwave water fraction retrieval algorithm (described in section 2.2). To estimate flood-potential, we derive a surface water flow-field from ~100m DEMs (upper right, see appendix F), accounting for hydrologically incorrect DEM features. We use the flow-field to map major drainage channels (lower left) exceeding a chosen threshold catchment size (expressed in pixels). Finally, we produce a prototype flood-potential database that merges elevation, flow-field, catchment size, land-use, historic flood extent, and FOV extent data (lower right).

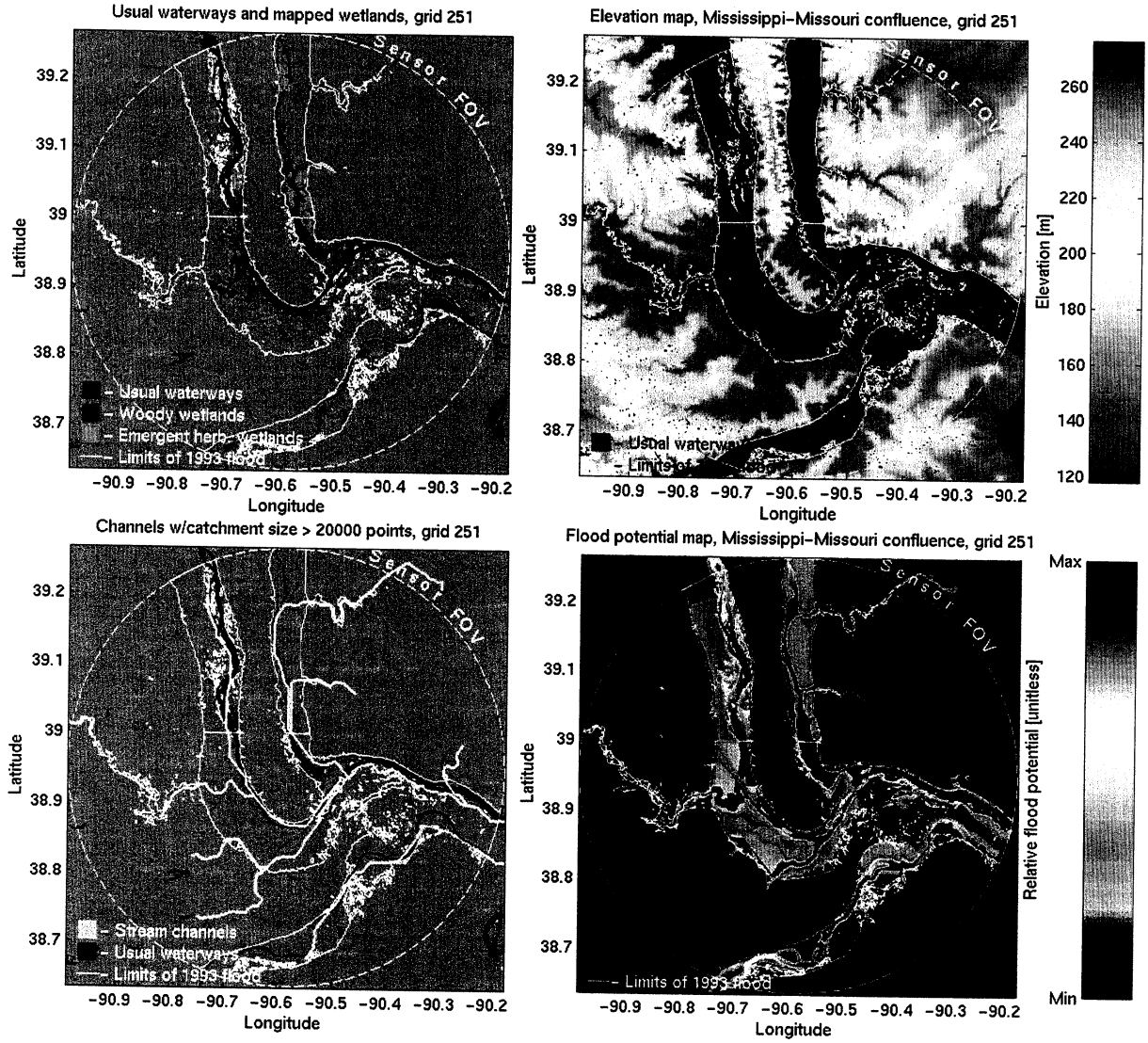

Figure 2-1: Maps showing data for flood-potential database derivation. Top left: USGS National Land Cover Data showing open water and wetlands. Top right: Elevation map from USGS 1:250,000 DEMs. Bottom left: Flow routing map (>20,000-point catchment sizes only). Bottom right: Derived prototype relative flood potential map.

The flood potential map must translate a scalar flood-fraction estimate into a two-dimensional flood map in real-time. We required that the potential map 1) be made from readily available data, 2) assign infinite potential (i.e., always wet) to stream channels with potential decreasing with altitude or distance away from the channels, and 3) allow nearly continuously varying flood-fraction. We derived any further design elements by trial and error using four diverse test cells within the larger study area. The flood potential software executes the following steps culminating in the flood potential map for a grid cell:

- *Iteratively determine flow routing through the cell using the elevation map*: Isolated flow "dead-ends"—local minima in the elevation map—are initially removed. Flow is then traced between neighboring pixels by finding the direction of steepest gradient. Flow must also be traced over larger "flat" regions of the elevation map. This is done for many flat points by iteratively finding those having neighboring points with outward flow and

assigning flow from the flat point to the nearest outward-flow point. We determine the flow through most remaining flat regions—for example, those behind real or artificial "dams" in the DEM—by raising the region over the obstacle and repeating the flow tracing process. Finally, we trace flow across any flat regions that terminate at the map edges.

- *Find stream channels*: Using the flow routing map, we determine the catchment size—or drainage area—of each point. We can then identify stream channels by choosing a minimum drainage area. Here we chose a 20,000-pixel threshold and deleted channels outside either the SAST maximum flood extent boundaries or the FOV.
- *Calculate the flood-potential relative to stream channels*: Channels are assigned infinite potential and (lower) potential must be assigned to the remaining points such that the potential map allows continuously varying flood-fraction levels. For each map point, we find the first stream channel point downhill then calculate the altitude difference (Δ_{alt}) and distance (d) between the point and the stream channel. The maximum distance $d_{max}(\Delta_{alt})$ among all points on the map with the same Δ_{alt} is also found. Then we calculate the flood potential of a map point as:

$$P = 1 / [\, \Delta_{alt} + d / d_{max}(\Delta_{alt}) \,]. \quad (1)$$

  That is, as flood-fraction increases, all points with the same Δ_{alt} are (virtually) inundated before points with the next larger Δ_{alt}; points with the same Δ_{alt} are inundated as a function of distance from the stream channel.
- *Determine what points on the rectangular map are within the sensor FOV*: Although FOVs mark merely the half-power (3dB) contour of a passive microwave sensor's two-dimensional spatial weighting pattern, weighting decreases rapidly beyond the FOV and most of the signal picked up by the sensor comes from within or just beyond the 3dB contour. We restrict the retrieval area to the 3dB contour to maximize spatial correspondence between retrieved flood-fraction and the flood-extent map derived from it.

2.2. Microwave flood-fraction algorithm

In order to minimize atmospheric effects, the algorithm includes a physical inversion module that estimates land surface emissivities (see appendix E). However, in tests with SSM/I data we have not found any evidence that the emissivity retrieval step improves flood-fraction accuracy beyond what can be derived from radiances alone. Since sounding channels should improve emissivity retrieval accuracy, further tests with SSMIS data will show how much sounding channels can improve flood-fraction retrievals.

The algorithm calculates flood-fraction from microwave data (radiances or emissivities) using a linear regression model (see appendix D). To calibrate the regression model, we would like to observe a range of flooded conditions simultaneously with both microwave and higher-resolution sensors (e.g. LandSat). For this study, we had only two points: 1) The SAST maximum flood extent map for maximum observed flood-fraction and 2) USGS National Land Cover Data (NLCD, http://landcover.usgs.gov/) for non-flood conditions. Since neither dataset is date-specific, we used 37 GHz H-pol. emissivity as a proxy for the timing of high and low water extents. That is, we calibrated the model by matching point 1 to the *lowest* 37H emissivity observed during the study period (June 21-August 9, 1993) and point 2 to the *highest* 37H emissivity observed during a control period (June 30-July 10, 1994). We calibrated the model

for the four channels at 19 and 37 GHz and took the average value for our flood-fraction estimate.

2.3. High-resolution flood mapping

The mapping process is relatively simple and quick: 1) Retrieve flood-fraction from microwave data (linear regression) and 2) iteratively solve for a flood potential that—when applied to the flood-potential map—gives a flood-fraction closest to that estimated from brightness temperatures. Given a potential value, the flood map consists of all points that either exceed the potential or are known from land surface classification data to be water. Only points within the sensor FOV are counted toward the total flood-fraction of the cell.

3. 1993 Great Midwest Flood Results

The 1993 Great Midwest Flood hit parts of nine states and lasted through much of the summer. Based on calculations with the SAST maximum flood extent map, there were ~760 EASE-Grid points (~25 km spacing) with flooding and ~21% of these had peak flood-fractions >0.1 (for 70 km FOVs). We have produced flood map animations covering 6/21-8/9 for four cells having 0.16-0.39 peak flood fractions. Appendix H provides flood-mapping examples for all four cells.

Figure 3-1 shows map sequence snapshots for the cell near the Mississippi-Missouri confluence along with the complete flood-fraction retrieval time series. The maximum flood extent overlay provides detailed spatial validation of the August 8 map. (The overlay should not be used as flood-fraction validation because it is also the source of algorithm peak-flood calibration data.) The two maps are well matched for most of the Miss. (river at top left of map), Illinois (top right), and Missouri flood plains and their tributaries.

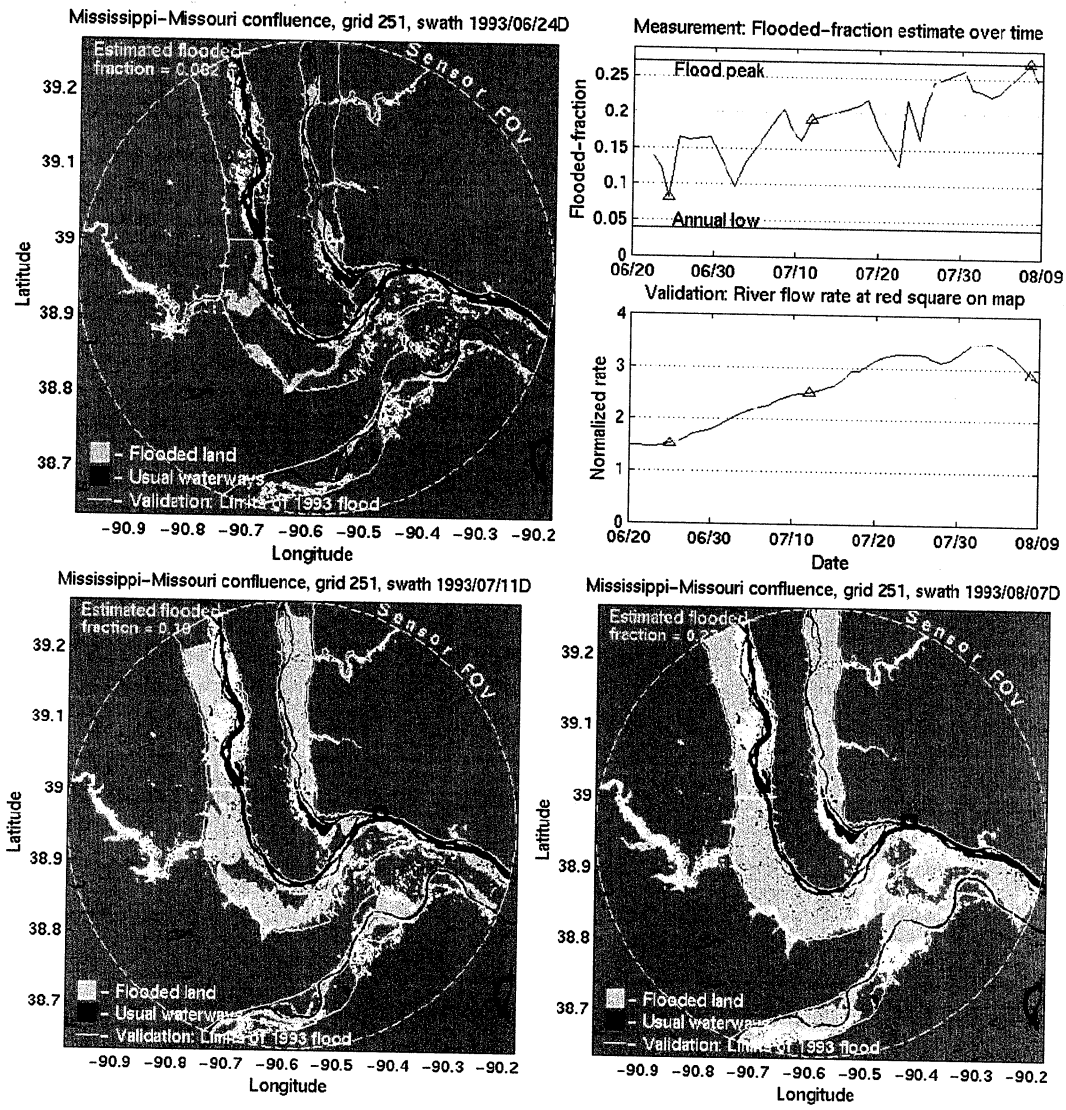

Figure 3-1: Snapshots of a real-time flood map sequence. Top: June 24, 1993. Bottom: July 11 and August 7. The maximum flood extent truth for 1993 Midwest Flood (solid white overlay) is a rough validation of the August 7 retrieval. The plots on the right show the evolution over time of the flood-fraction estimate and river flow rates measured at the red square on the maps; the triangles mark the dates mapped.

Comparison to the river discharge time series (Figure 2-1, lower line plot, see appendix B) suggests that the flood-fraction retrieval is capturing the temporal trend with ~0.05 error variance. (For comparison, tests of water-fraction retrieval with global datasets gave 0.1 RMSE.) The apparent magnitude of the error variance is similar to that found in the other test cells and seems to be independent of the flood-fraction. We tested the effect of randomly oriented, oval footprint sampling using the true flood maps and found that random orientation alone could cause 0.03-0.05 flood fraction retrieval standard error. Implementation of circularized footprint matching should remove much of this error.

4. Discussion

The 1993 tests demonstrate the feasibility of the mapping method and help pinpoint areas where it needs to be improved. For example, the mapping method assumes that each basin in the FOV

is subject to similar amounts of flooding. (This was the case in the example above but not in all the test cells included in appendix H.) To improve map accuracy when this assumption is invalid, we plan to use stream flow data (when available) to scale flood levels separately in each basin while simultaneously matching the mapped flood-fraction to the microwave retrieval.

To produce useful real-time flood maps, the flood-fraction retrieval error needs to be small relative to the total flood-fraction of the retrieval cell. If errors are independent of the flood-fraction, then the effective signal-to-noise level decreases with flooded area, minimizing the usefulness of the retrieval for floods much smaller than the sensor FOV. Therefore, both flood-fraction retrieval accuracy and FOV size improvement are important for improving flood map accuracy and robustness for smaller floods. Planned sensors will have improved FOV sizes (e.g., CMIS 19 GHz FOV will be <25 km). With SSM/I, we can lower FOV size by using only the 37 GHz channels (37 km FOV) but lose any chance for atmospheric correction. In future work, we plan to run tests with SSMIS to determine an optimal balance between atmospheric correction skill and spatial resolution.

5. Conclusion

We have developed a prototype real-time flood mapping method that transforms low-resolution passive microwave estimates of flood-fraction into high-resolution flood maps. Feasibility study results from the well-documented 1993 Great Midwest Floods demonstrate the method's ability to make dynamic flood maps over long time periods. Mapping error, which is dominated by flood-fraction retrieval error, must be improved to meet most user needs. Algorithm refinements (e.g., footprint circularization, adjacent cell smoothing) should provide some immediate improvement while we wait for planned sensor advances (e.g., better spatial resolution, atmospheric sounding channels). Other planned enhancements include adaptations for Shuttle Radar Topography Mission DEMs (discussed in appendix I), estimation of river stage, incorporation of *in situ* river stage data, and improved calibration against available high-resolution imagery.

We have presented this research at IGARSS'02 in Toronto, Canada, June 29, 2002 and a version of the above material was published in the conference proceedings [6]. The Appendix provides more details on the research including flood-mapping examples from all four EASE-Grid cells examined.

6. References

[1] S. J. Sippel, S. K. Hamilton, J. M. Melack, and B. J. Choudhury, "Determination of inundation area in the Amazon River floodplain using the SMMR 37 GHz polarization difference," *Rem. Sens. Env.*, 48:70-76, 1994.

[2] S. K. Hamilton, S. J. Sippel, and J. M Melack, "Inundation patterns in the Pantanal wetland of South America determined from passive microwave remote sensing," *Archiv fur Hydrobiologie*, 137(1):1-23, 1996.

[3] S. J. Sippel, S. K. Hamilton, J. M. Melack, and E. M. M. Novo, "Passive microwave observations of inundation area and the area/stage relation in the Amazon River floodplain," *Int. J. Rem. Sens.*, 19(16):3055-3074, 1998.

[4] R. L. Armstrong and M. J. Brodzik, "An Earth-Gridded SSM/I data set for cryospheric studies and global change monitoring," *Adv. Space Res.*, 16(10):155-163, 1995.

[5] C. D. Rodgers, "Retrieval of atmospheric temperature and composition from remote measurement of thermal radiation," *Rev. Geophys.*, 14:609-624, 1976.

[6] J. F. Galantowicz, "High-resolution flood mapping from low-resolution passive microwave data," *Proc. IGARSS02,* Toronto, pp. 1499-1502, 2002.

APPENDIX

A. Flood extent dataset

Figure A-1 shows a map of maximum flood extent for the 1993 Midwest Flood acquired from SAST (Scientific Assessment and Strategy Team, http://edcwww2.cr.usgs.gov/sast-home.html). The map consists of polygons that enclose flooded regions as well as polygons enclosing "islands" and open water within the islands. The SAST project derived the map from high-resolution imagery (i.e., LandSat and SAR) acquired around the time of maximum flooding at St. Louis (July 12, 1993 or day 193). We originally sought to acquire flood imagery for a range of times to provide a long baseline period against which to calibrate water fraction retrievals from brightness temperatures. Although this remains a goal for future work, success hinges on the acquisition of multiple radar images (probably from more than one platform) because persistent cloudiness usually obscures the surface during long-term flood events.

We developed tools (in Matlab) for reading the flood extent dataset and calculating the amount of open water present in 70 km circles approximating the effective "footprints" of SSM/I brightness temperature data. Because of the size, quality, and complexities of the SAST flood extent dataset, considerable time was required to devise quality control checks and process the all the data. Figure A-2 shows the fractional area of floodwater coverage at each of the grid points. (Points with zero water coverage and those near the edge of the SAST analysis region are excluded.) The maximum coverage is about 0.4 and most cells (82%) have less than 10% coverage.

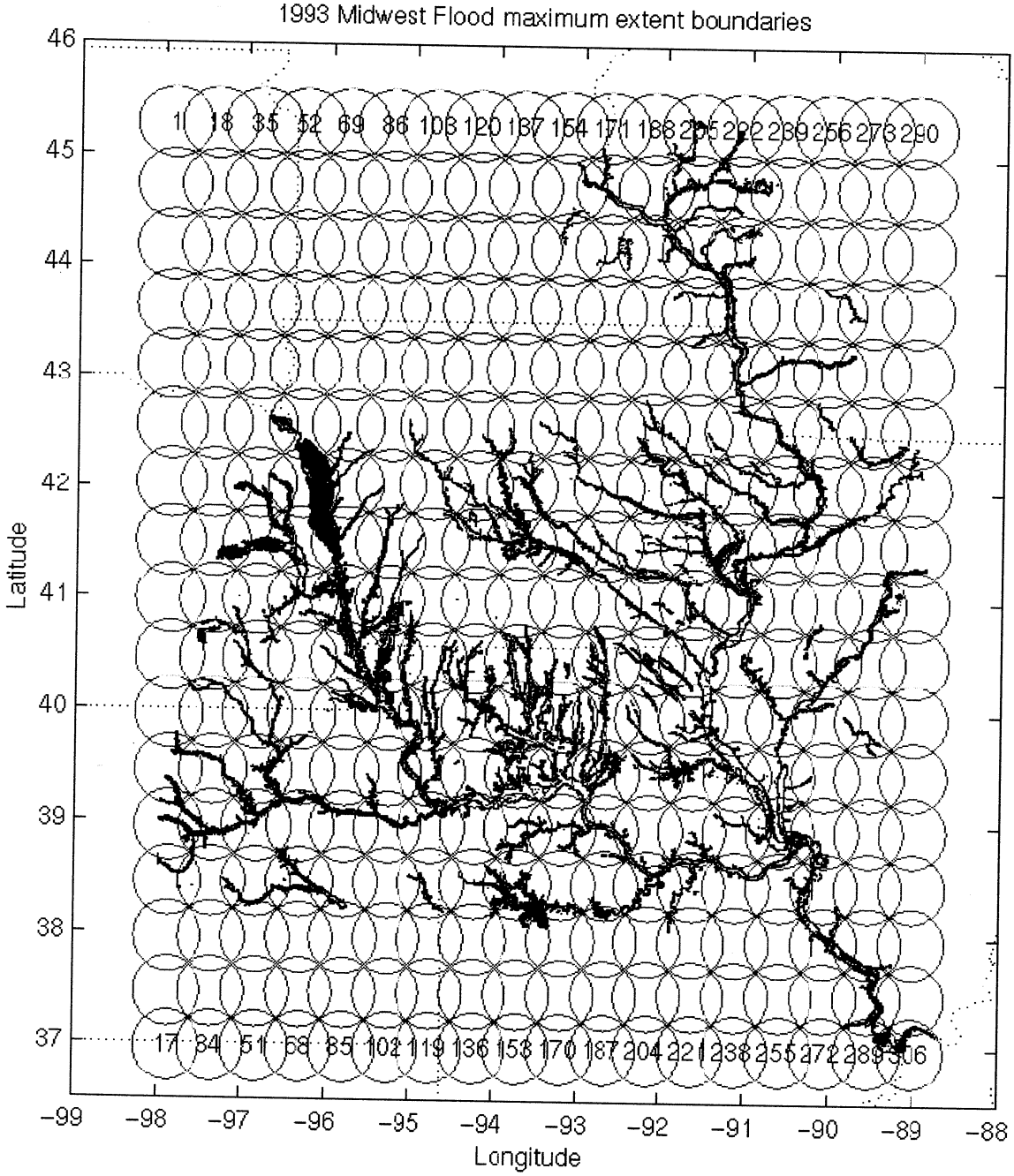

Figure A-1: Map of maximum flood extent boundaries from high-resolution imagery analysis. 70 km diameter circles correspond to EASE-Grid brightness temperatures.

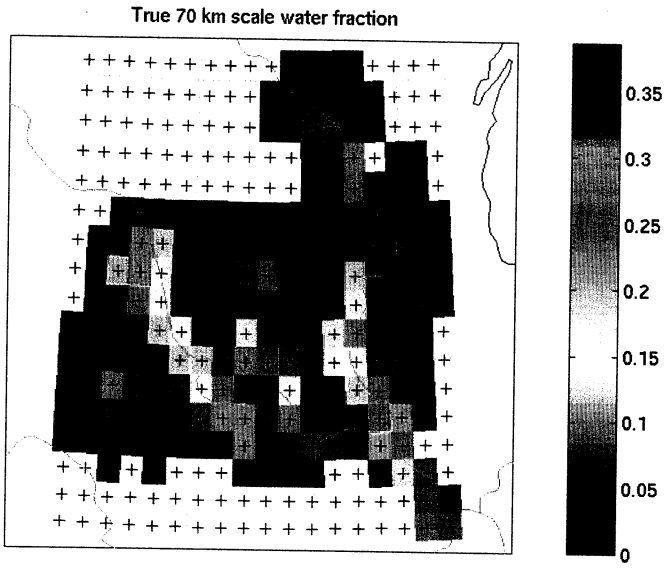

Figure A-2: Water fraction derived from flood extent map (above) in 70 km diameter circles at EASE-Grid locations.

B. Peak flood timing from stream flow data

We acquired daily stream flow (discharge) data from the US Geological Survey (URL: http://water.usgs.gov/nwis/discharge) for 17 sites covering 1992-1994: 10 sites on the Missouri river and 7 on the Mississippi, one of which was below the Mississippi-Missouri confluence. Figure B-1 and Figure B-2 plot the discharge rates over time. Note from Figure B-2 that the dates on which maximum discharge (and, presumably, maximum flood extent) occurred vary considerably among the gauging stations. We plot the date of maximum discharge as a function of drainage area in Figure B-3. The flood-extent map from SAST (described above) relies primarily on LandSat imagery requiring cloud-free conditions. Given the persistence of clouds during the flood and the wide range of peak-flood dates, it is likely that the SAST map underestimates the true maximum flood extent somewhat. (Except where near-continuous coverage is possible, it is likely that *any* remotely-sensed flood-imagery would underestimate maximum extent because of the difficulty of capturing images at just the right time.) However, since the SAST data is currently the only high-resolution map we have available for the 1993 flood, we assumed that it is an accurate representation of the true maximum flood extent, albeit with no clear identification of peak flood timing. In appendix D we discuss how microwave emissivities were used to get approximate peak flood timing for each retrieval cell.

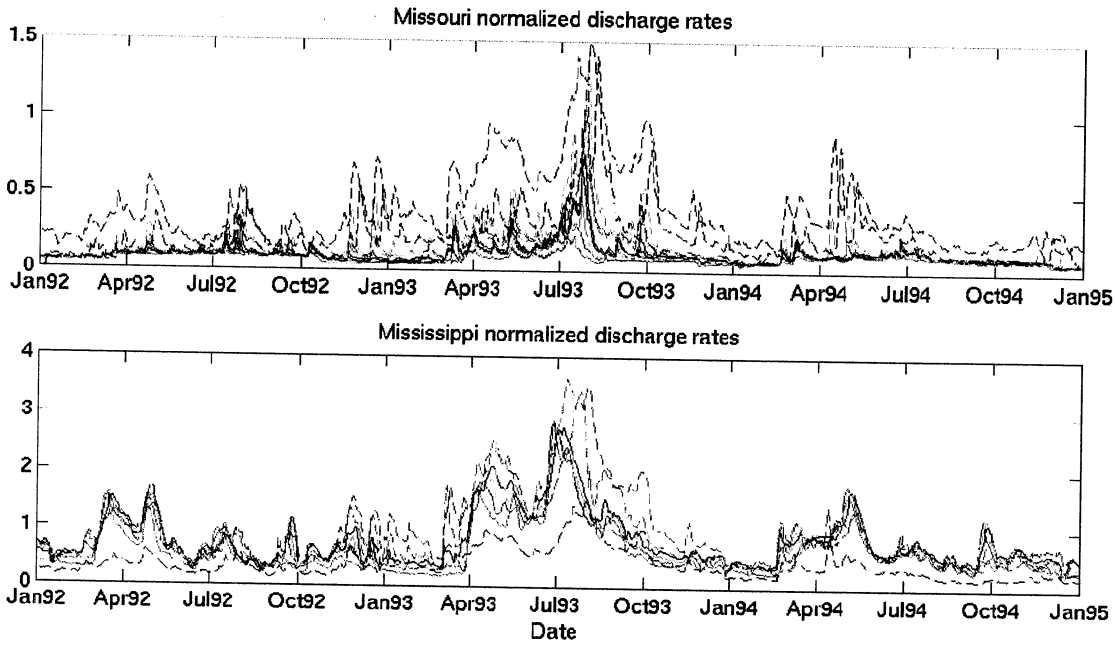

Figure B-1: 1992-1994 river flow (discharge) rates at USGS gauging station sites on the Missouri (top) and Mississippi rivers. Rates are normalized by the drainage area reported for each site.

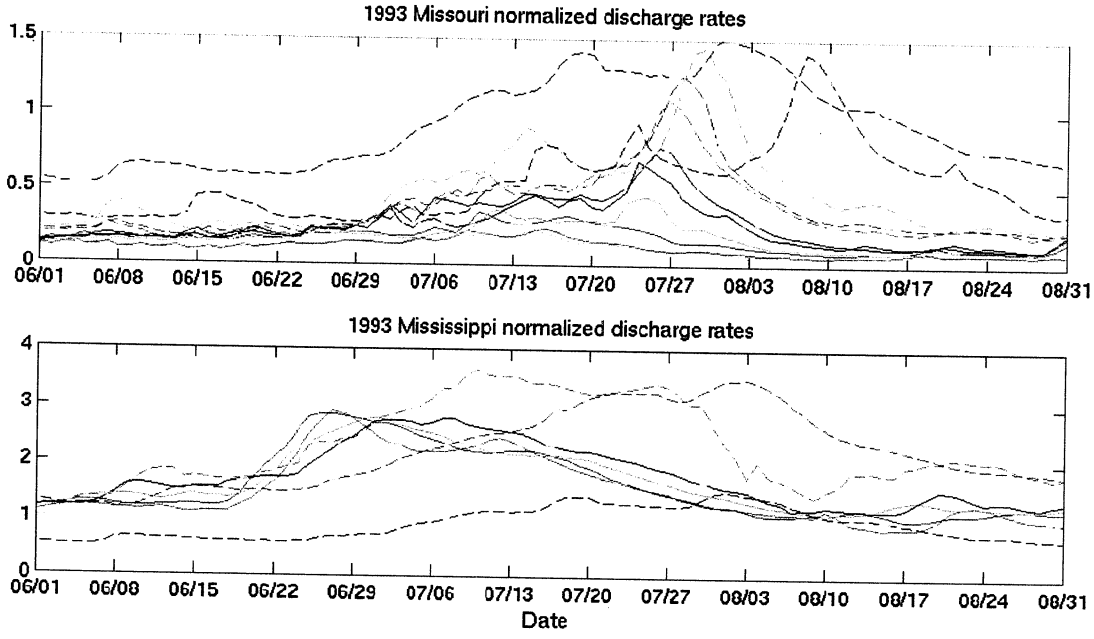

Figure B-2: Same as Figure B-1 but for 1993/06/01-1993/08/31.

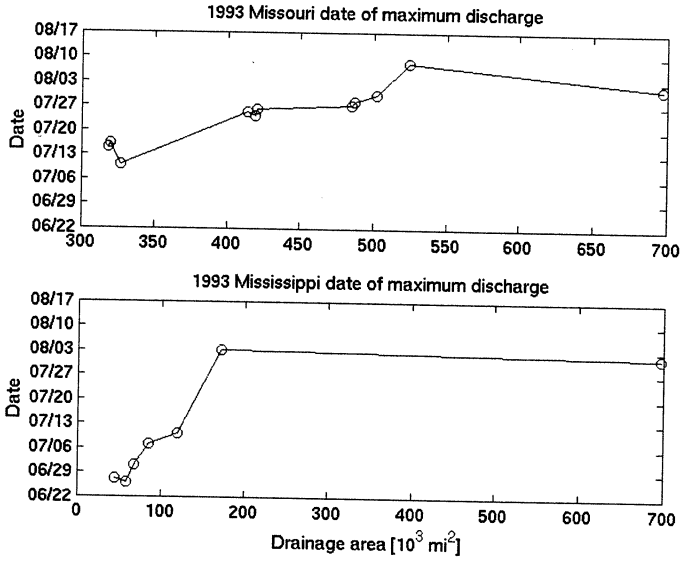

Figure B-3: Date of maximum river discharge as a function of drainage area for sites on the Missouri (top) and Mississippi rivers. The site at 700,000 mi^2 is below the Mississippi-Missouri confluence and is shown on both plots.

C. Dry-season water coverage

To calibrate the relationship between microwave observations and areal flooded-fraction (discussed in appendix D) we would like to observe a range of flooded conditions with both microwave and high-resolution sensors (e.g. LandSat) simultaneously. The SAST maximum flood extent map provides one calibration point at maximum observed flooded-fraction. We took a second point from USGS National Land Cover Data (NLCD) state-by-state maps (URL: http://landcover.usgs.gov). We have developed Matlab software for ingesting NLCD data, merging maps that cross state lines, and registering the data to USGS 1:250,000 scale digital elevation models (discussed in appendix F). Figure C-1 shows a map of NLCD water-related types with the nominal 70 km EASE-Gridded SSM/I field-of-view and the SAST maximum extent map overlaid. Future work should include analysis of multiple high-resolution images of the 1993 flood in order to evaluate errors and reduce reliance on these two datasets.

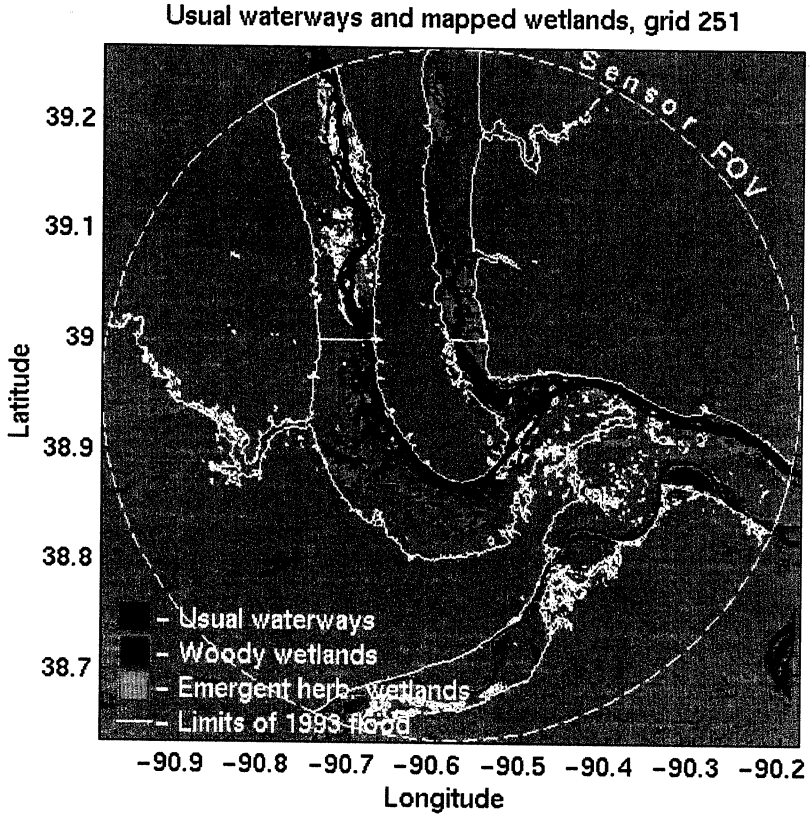

Figure C-1: Example USGS National Land Cover Data showing open water, woody wetlands, and emergent herbaceous wetlands surface types near the Mississippi-Missouri River confluence. Also plotted is the outline of an EASE-Gridded 70 km SSM/I sensor FOV and the 1993 flood limits from the SAST map.

D. Flooded-fraction calibration

To retrieve flooded-fraction from radiometric measurements (either emissivities or TBs as discussed in appendix E) we used a simple two-point calibration for each grid cell.

- For point one, we matched the flooded-fraction calculated from the SAST maximum flood extent map to radiometric measurements corresponding to the *lowest* 37 GHz H-pol. emissivity estimated during the study period (June 21-August 9, 1993). That is, we used the 37H emissivity as a proxy for maximum flood extent timing. As shown in Figure E-1 and Figure E-2, below, there was fairly good correspondence between peak-flood timing from this method and peak stream flow timing. The advantage of this method is that the maximum flooded-fraction that we can retrieve from brightness temperatures will be approximately limited to that of the SAST maximum flood extent map.
- For the second point, we matched the fraction of known waterways in the cell from NLCD land classification data to radiometric measurements corresponding to the *highest* 37H emissivity estimated during a known dry period (June 30-July 10, 1994). We chose this time span because vegetation characteristics should have been similar to the flood study period and stream flow rates were near their 3-year low (see Figure B-1).

Given these calibration points, the retrieval software uses a simple linear model to calculate flooded fraction from a single-channel radiometric measurement. In our flood mapping tests (section 3 and appendix H) the estimated flooded-fraction is the average of calculations from

19V, 19H, 37V, and 37H data. However, there were insignificant differences between the average and flooded-fraction calculated from 19H emissivities alone.

E. Derivation of emissivity from brightness temperature

Flooded-fraction within a radiometer's field-of-view affects the brightness temperature measurement primarily through its influence on surface emissivity. In order to isolate emissivity changes from the overall variability in brightness temperature over time, we applied a physical retrieval algorithm to SSM/I brightness temperatures (e.g., [5]). The algorithm uses an atmospheric radiative transfer model to derive a solution state that is statistically consistent with *a priori* physical constraints and the measurements in a least-squares sense. The retrieval model surface is described by a single emitting temperature variable and a spectral emissivity vector. Although the SSM/I channel set—19V/H, 22V, 37V/H, and 85V/H—is not well suited to a full physical inversion because of the lack of a complete atmospheric sounding channel set, the physical inversion has the advantage that no special adjustments or calibration are needed to adapt to dramatically changing emissivity conditions. In contrast, an empirical-regression type algorithm would require simultaneous calibration against both local temperature and emissivity or flood extent data—a significant burden since most flood events are too short-lived and cloud-obscured to provide sufficient calibration data of this type.

Figure E-1 and Figure E-2 below illustrate the difference in flooded-fraction evolution over time when emissivity is used in place of brightness temperature (TB). For both input types, flooded-fraction is calculated from a linear model calibrated at low (dry-season) and presumed flood-peak points (discussed in appendix D above). Although emissivity-based flooded fraction clearly differs from TB-based, both follow the observed flood trend (represented by river flow data) and both show approximately 0.05 variability around the trend. There is no way to independently verify the flooded-fraction retrievals at this time because only one flood extent map is available and this map provides our "flood-peak" calibration data.

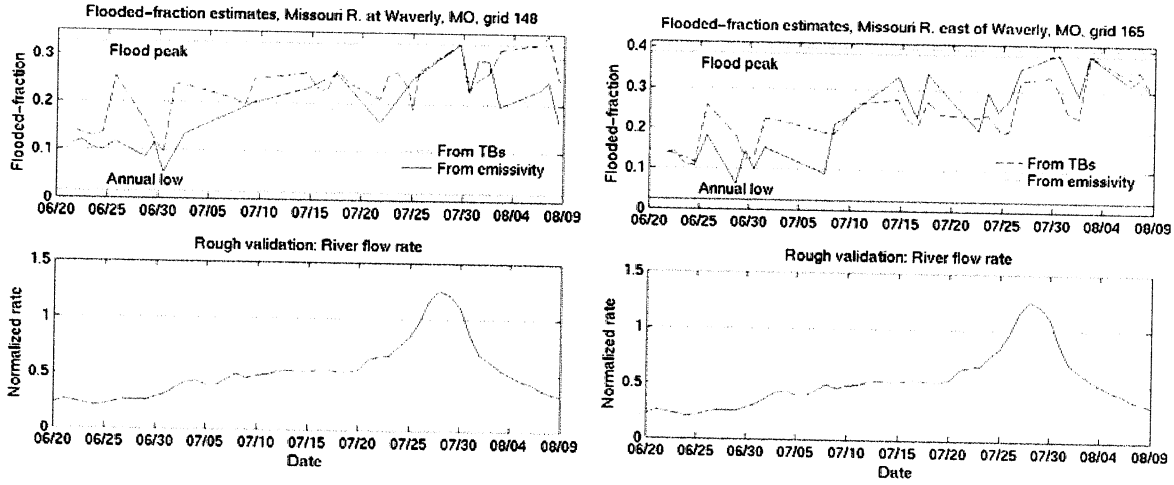

Figure E-1: Comparisons of TB- and emissivity-derived flooded fraction evolution (top plots) for grid cells 148 and 165. Bottom plots are river flow rates measured in or near each grid cell.

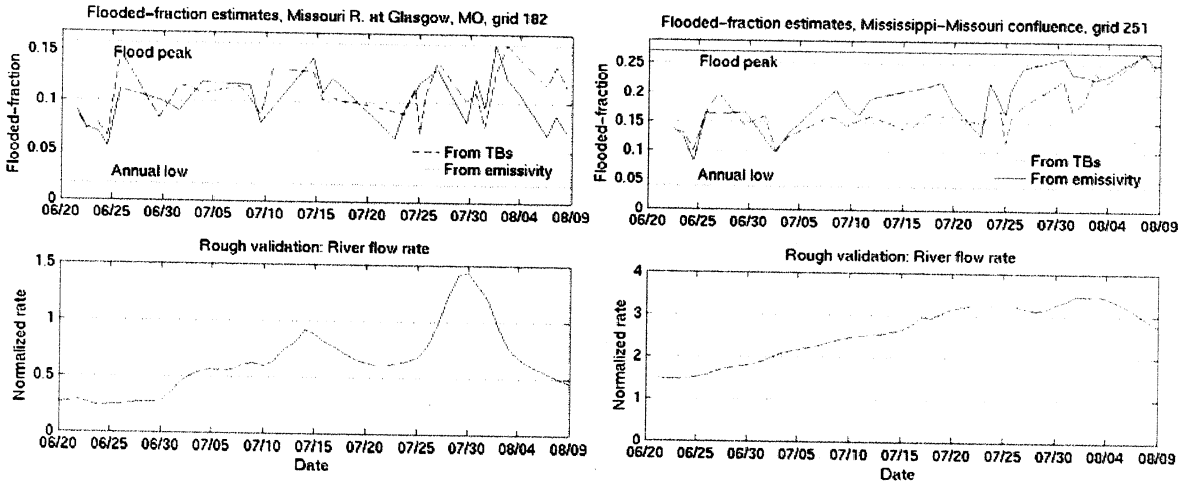

Figure E-2: Same as above but for grid cells 182 and 251.

F. USGS 1:250,000 Digital Elevation Models

Our flood-mapping method uses high-resolution digital elevation models (DEMs) to create a map of flood-potential that translates a flooded-fraction measurement to a two-dimensional map (see appendix G). The nominal spatial resolution of the flood mapping method is limited only by the resolution of the DEM used. Of course, the spatial accuracy of the flood map is a function of errors in the flooded-fraction retrieval and the assumptions of the mapping methodology itself. We chose to use the ~100 m resolution USGS 1:250,000 DEM (URL: ftp://edcftp.cr.usgs.gov/pub/data/DEM/250) because it is more readily accessible and usable (i.e., small dataset size) than higher-resolution DEMs while at this resolution horizontal errors are still relatively small compared to other error sources in our flood-mapping method. Figure F-1 shows an example elevation map of the study grid cell near the Mississippi-Missouri confluence (grid cell 251).

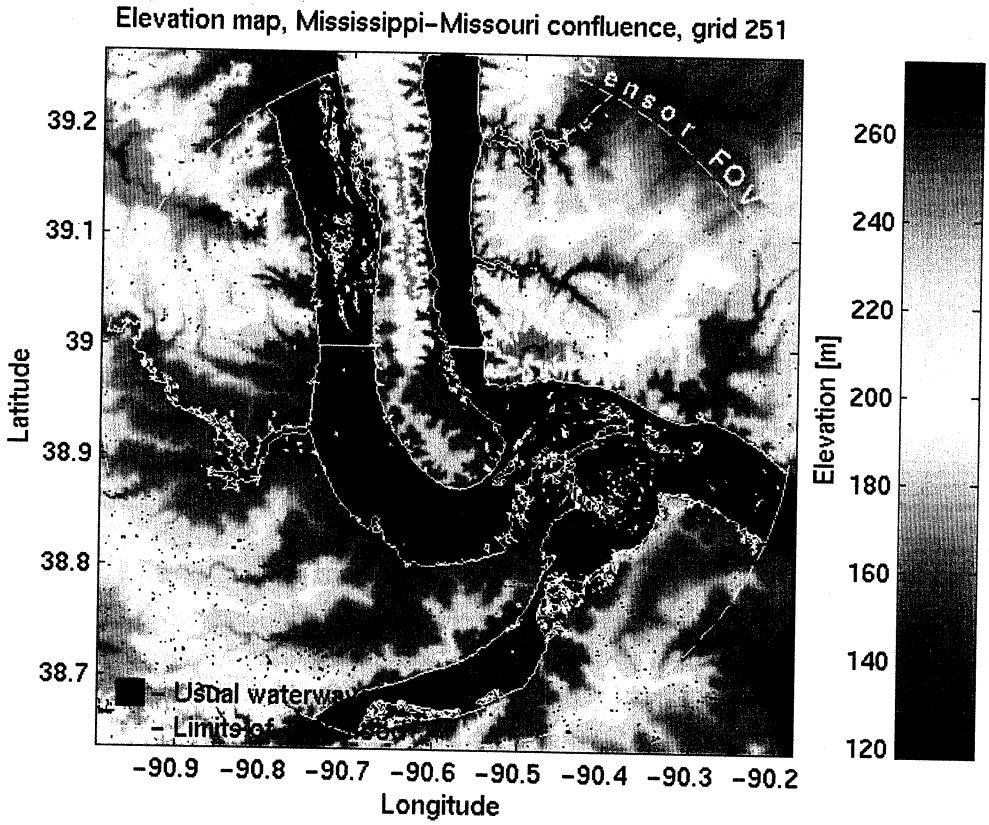

Figure F-1: Example elevation map made from USGS 1:250,000 DEMs. Up to four individual 1-degree square DEMs are merged and cropped to the size of the brightness temperature FOV. Also plotted is the outline of an EASE-Gridded 70 km SSM/I sensor FOV and the 1993 flood limits from the SAST map.

G. Prototype flood potential map

We have developed a prototype flood potential map that translates the scalar flooded-fraction measurement to a two-dimensional flood map in real-time. We required that the potential map 1) be made from available data (i.e., DEMs, historical flood maps, and land classification data), 2) assign infinite potential to stream channels with potential decreasing as altitude or distance increases away from channels, and 3) allow nearly continuously-varying flooded-fraction. We derived any further design elements by trial and error using four diverse test cells within the larger study area. The flood potential software executes the following steps culminating in the flood potential map for a grid cell:

1. Iteratively determine flow routing through the cell using the elevation map. Isolated flow "dead-ends"—local minima in the elevation map—are initially removed. Flow is then traced between neighboring pixels by finding the direction of steepest gradient. Flow must also be trace over larger "flat" regions of the elevation map. This is done for many flat points by iteratively finding those having neighboring points with outward flow and assigning flow from the flat point to the nearest outward-flow point. We determine the flow through most remaining flat regions—for example, those behind real or artificial "dams" in the DEM—by raising the region over the obstacle and repeating the flow tracing process. Finally, the software traces flow across any flat regions that terminate at the map edges.

2. Using the flow routing map, determine the catchment size—or drainage area—of each point.
3. Find stream channels. We tried a variety of methods for determining an optimal set of channels for the flood mapping application. The one that worked best in test cases took only points that had at least a 20,000-point catchment size and were inside the boundaries of the SAST maximum flood extent map. See Figure G-1 below.
4. Calculate the flood-potential relative to stream channels. Identified channels are assigned the highest (i.e., infinite) potential and other points have lower potential. The method chosen gave good test results and satisfied our requirement that the potential map allow continuously varying flooded-fraction levels. (See examples in Figure G-2 below). The method finds the stream channel point associated with each map point then calculates the altitude difference (Δ_{alt}) and distance (d) between the point and the stream channel. The maximum distance $d_{max}(\Delta_{alt})$ among all points on the map with the same Δ_{alt} is also found. Then we calculate the flood potential of a map point as:

$$P = 1 / [\, \Delta_{alt} + d / d_{max}(\Delta_{alt}) \,]$$

   As flooded-fraction increases, all points with the same Δ_{alt} become inundated before points with the next larger Δ_{alt} and points with the same Δ_{alt} are inundated as a function of distance from the stream channel.
5. Determine what points on the rectangular map are within the elliptical sensor FOV. Although FOVs mark merely the half-power (3dB) contour of a passive microwave sensor's two-dimensional spatial weighting pattern, weighting decreases rapidly beyond the FOV and most of the signal picked up by the sensor comes from within or just beyond the 3dB contour. We restrict the retrieval area to the 3dB contour to maximize spatial correspondence between retrieved flooded-fraction and the flood-extent map derived from it.

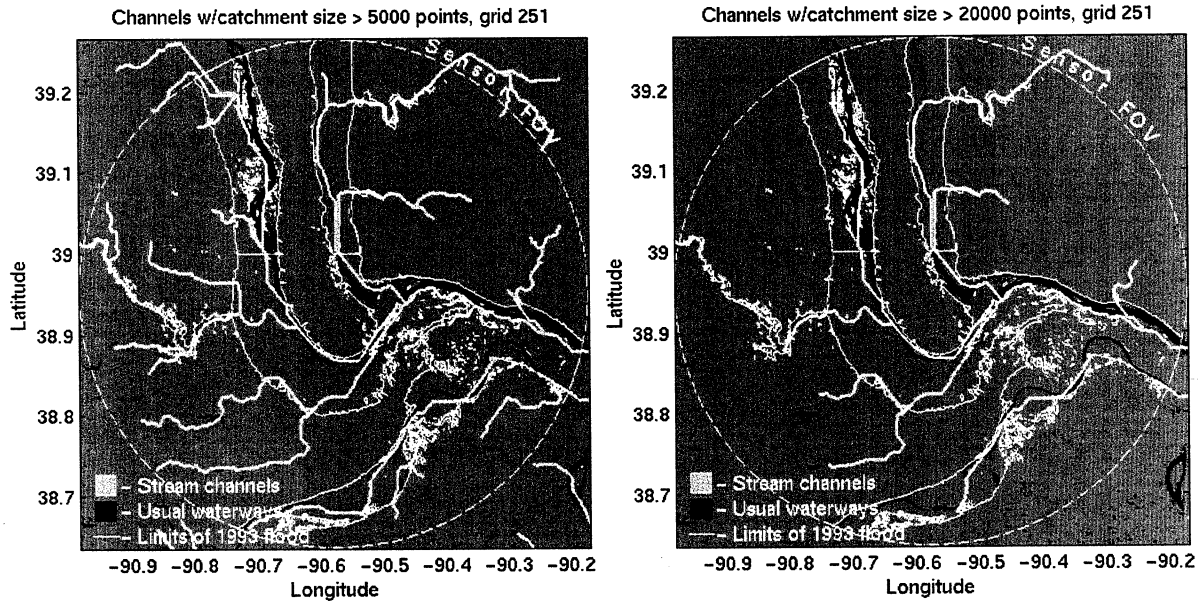

Figure G-1: Example maps showing channels with at least 5,000- (left) and 20,000-point catchment sizes.

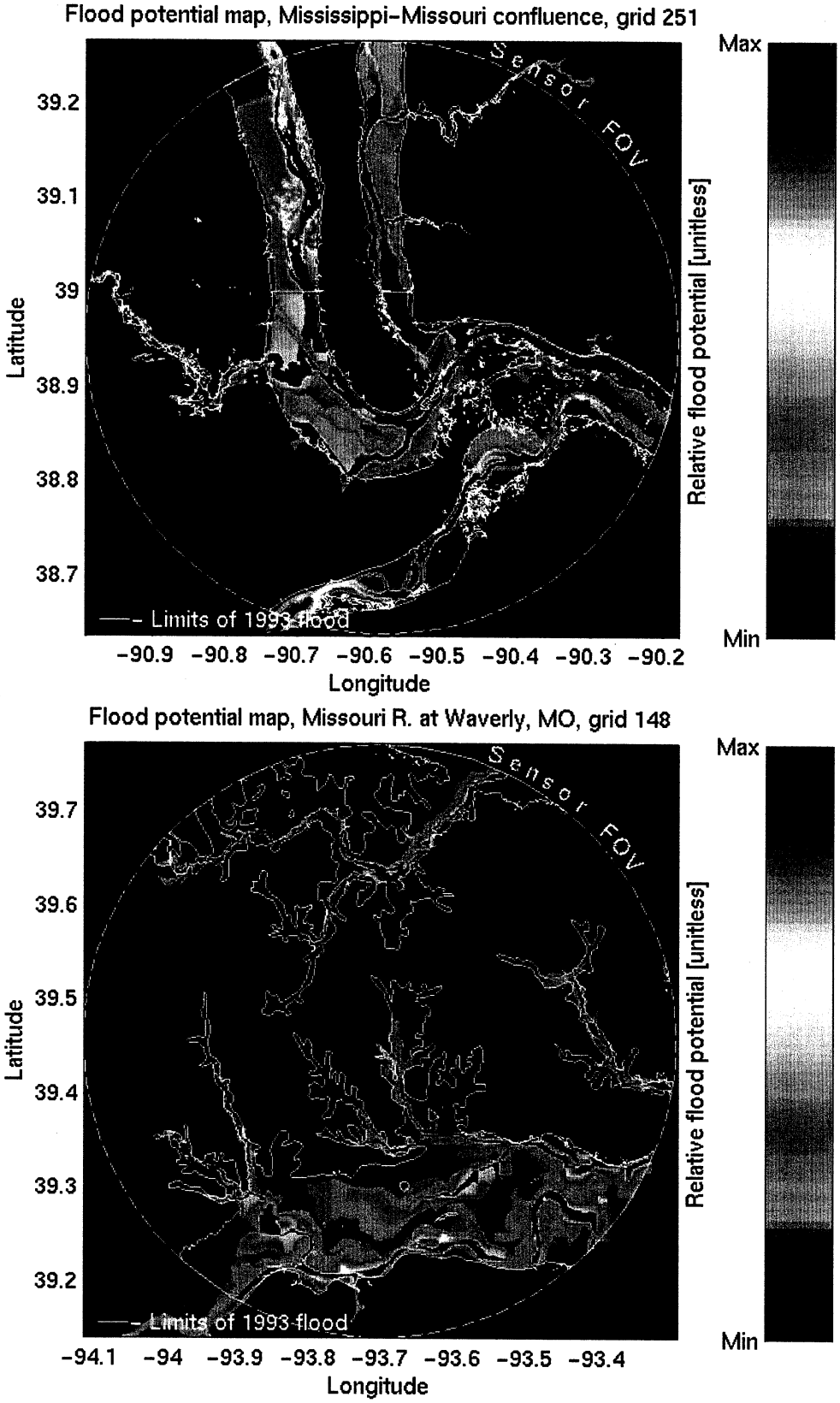

Figure G-2: Flood potential maps for study region grid points 251 (top) and 148 (bottom).

Although we believe based on the test cases below that the flow tracing processes we have developed are sufficient for flood-mapping applications, alternative methods and software packages should be considered in future work. For example, TOPAZ (Topographic Parameterization Software) is offered by the GrazingLands Research Laboratory, Agricultural Research Service, US Department of Agriculture (URL http://grl.ars.usda.gov/topaz/topaz1.htm). TOPAZ may provide beneficial features—including faster processing speeds—but there was insufficient time in this study to learn to use and adapt the program to the flood-potential problem.

H. Flood maps from flooded-fraction retrieval sequences

We can retrieve flooded-fraction from brightness temperature measurements any time observations are available and precipitation rates are minimal. (We check for the presence of precipitation both with a brightness temperature threshold test and with convergence criteria incorporated in the emissivity retrieval algorithm.) So far, we have made flood maps for four grid cells within the larger study area of the 1993 Midwest Flood. The maps cover the period from June 21-August 8, 1993 for up to 33 retrievals per grid cell. The mapping process is relatively simple and quick: 1) Retrieve flooded-fraction from brightness temperatures, as described in appendix D, and 2) iteratively solve for the threshold flood potential that gives a flooded-fraction closest to that estimated from brightness temperatures. Given a threshold potential, the flood map is made by flagging all points that either have a flood potential above the threshold or are known from land surface classification data to be water. Only points within the sensor FOV are counted toward the total flooded-fraction of the cell.

The figures below show example retrieval sequences for each of the four test cells. We have also created computer animations covering the full range of dates and showing the gradual evolution of the flood map in each cell.

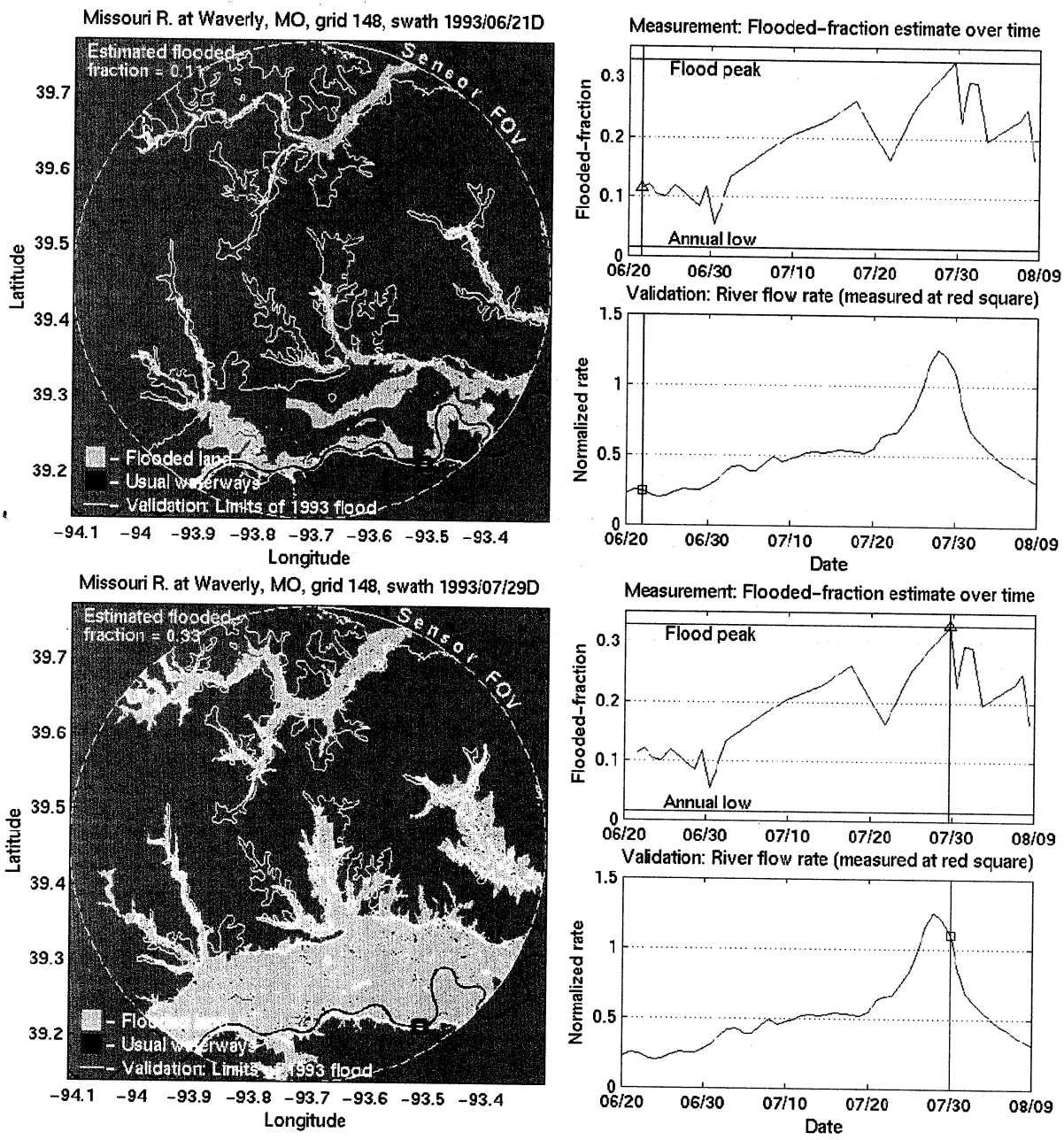

Figure H-1: Flood map sequence for grid cell 148 showing June 21 (top set) and maximum retrieved flooded fraction on July 29 (bottom). The maps include the SAST maximum flood extent boundaries for validation. The plots on the right show the evolution over time of the flooded-fraction estimate (top) and river flow rates measured at the red square on the map (bottom).

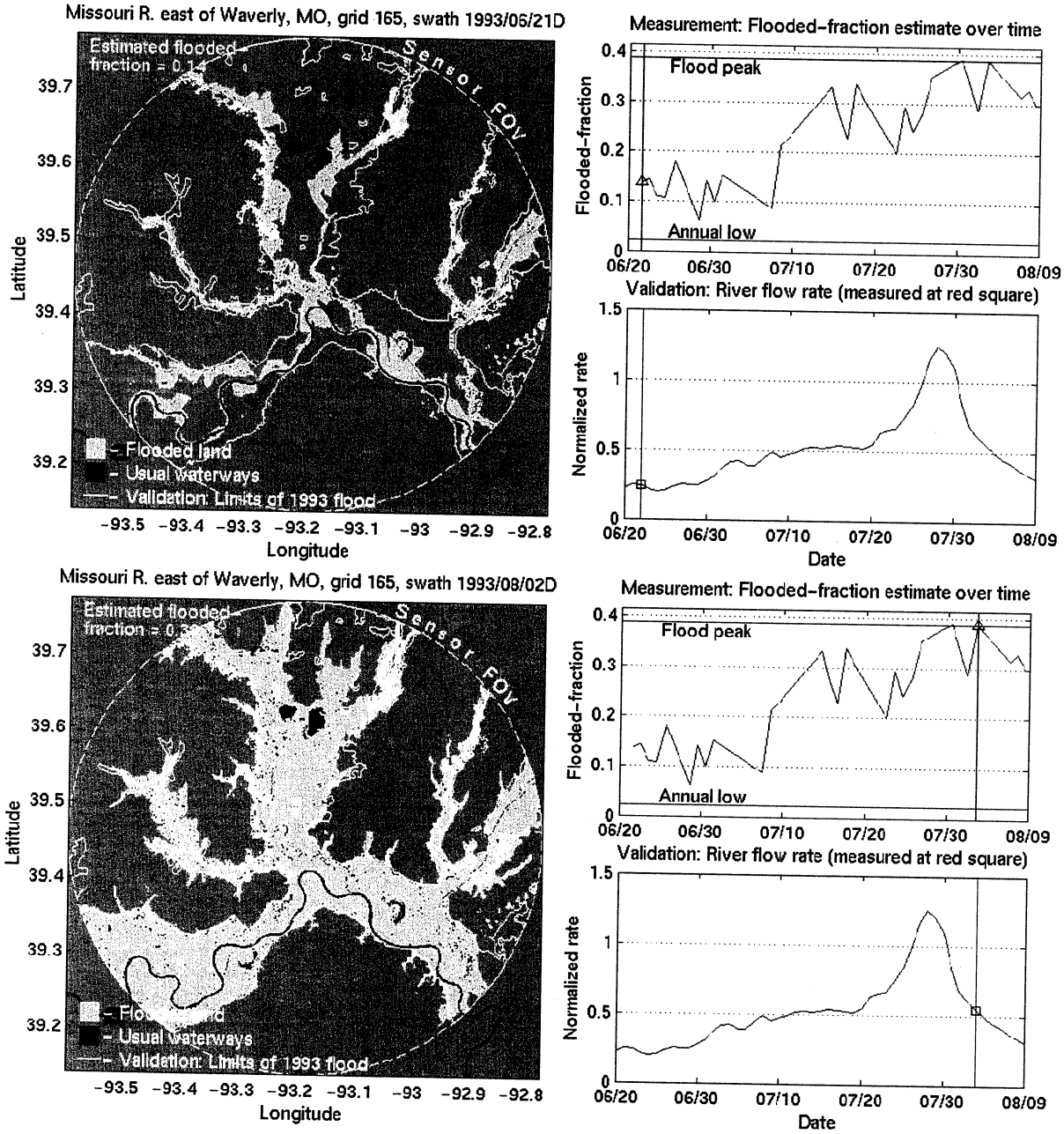

Figure H-2: Flood map sequence for grid cell 165 showing June 21 (top set) and maximum retrieved flooded fraction on August 2 (bottom). See Figure H-1 for description.

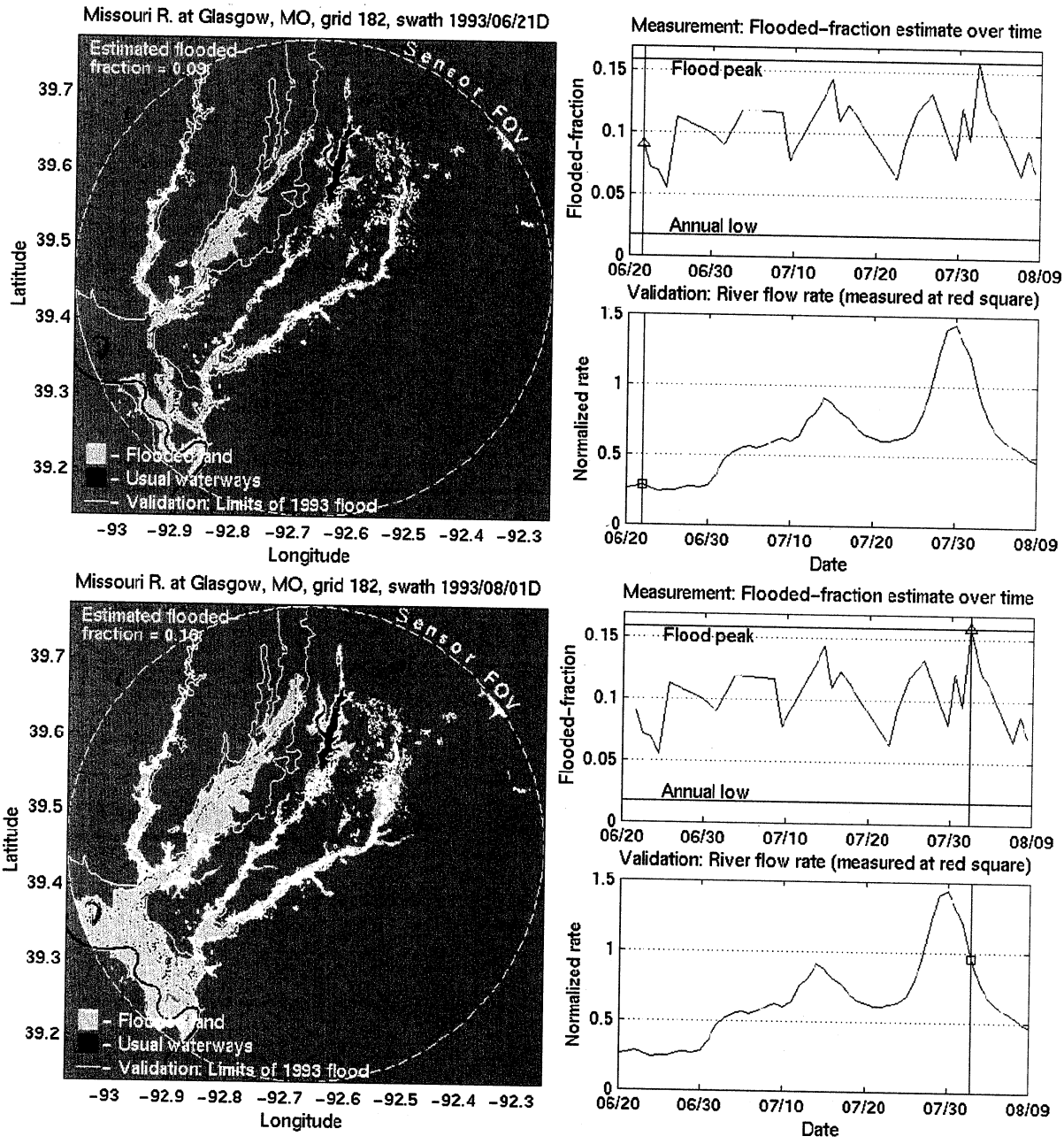

Figure H-3: Flood map sequence for grid cell 182 showing June 21 (top set) and maximum retrieved flooded fraction on August 1 (bottom). See Figure H-1 for description.

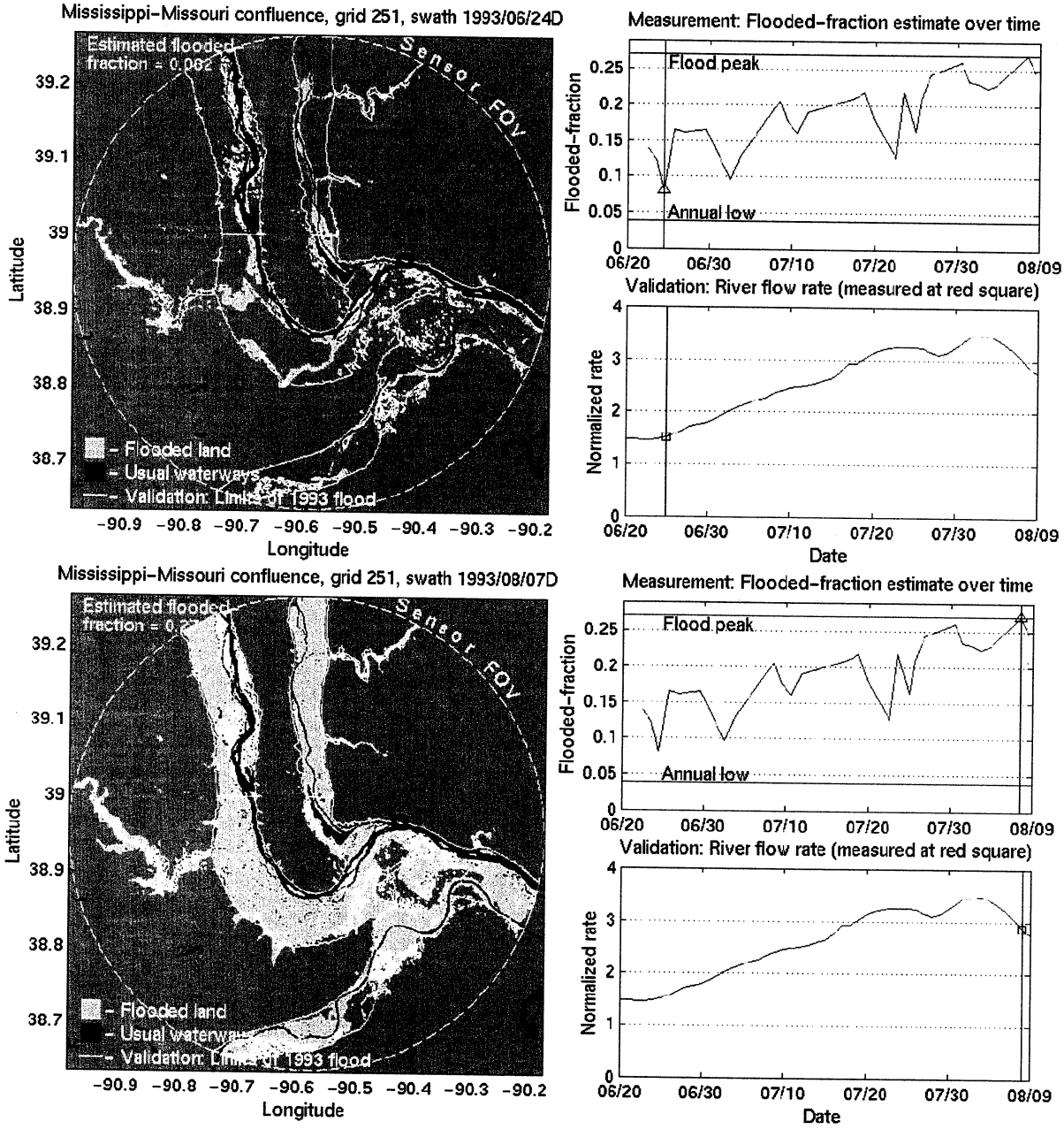

Figure H-4: Flood map sequence for grid cell 251 showing June 24 (top set) and maximum retrieved flooded fraction on August 7 (bottom). See Figure H-1 for description.

I. Shuttle Radar Topography Mapping Mission data

The Shuttle Radar Topography Mapping Mission (SRTM, http://www.jpl.nasa.gov/srtm) collected interferometric SAR (INSAR) data during a single Space Shuttle flight in Feb. 2000. Processing of the global raw data set to produce topographic data is ongoing. The PI of this project was assigned to the SRTM Science Team and given early access to designate small regions for DEM processing. We requested processing of the 1°x1° cells covering our grid cell 251 at the Mississippi-Missouri confluence. We merged the cells and cropped them to a region around the SSM/I EASE-Grid grid cell center (Figure I-1 below). The DEM's nominal resolution of 30 m is better than the ~100 m resolution of the USGS DEM described in appendix F. Also, we cropped the DEM to increase the map size by 40% over the nominal FOV size after

observing that the flood potential database could be improved by including catchment areas beyond the boundaries of FOV. We applied our flood potential algorithm (appendix G) to the SRTM DEM but were unable to produce a realistic flow-field such as that obtained with the USGS DEM (Figure G-1). We have not made further attempts to analyze the DEM to determine the cause of the failure. The SRTM DEM contained a significant number of processing artifacts including below sea-level points and random noise; water bodies were especially poorly mapped because of their low radar reflectivity. Further examination of the SRTM DEMs is warranted after the SRTM and NIMA teams have resolved these problems.

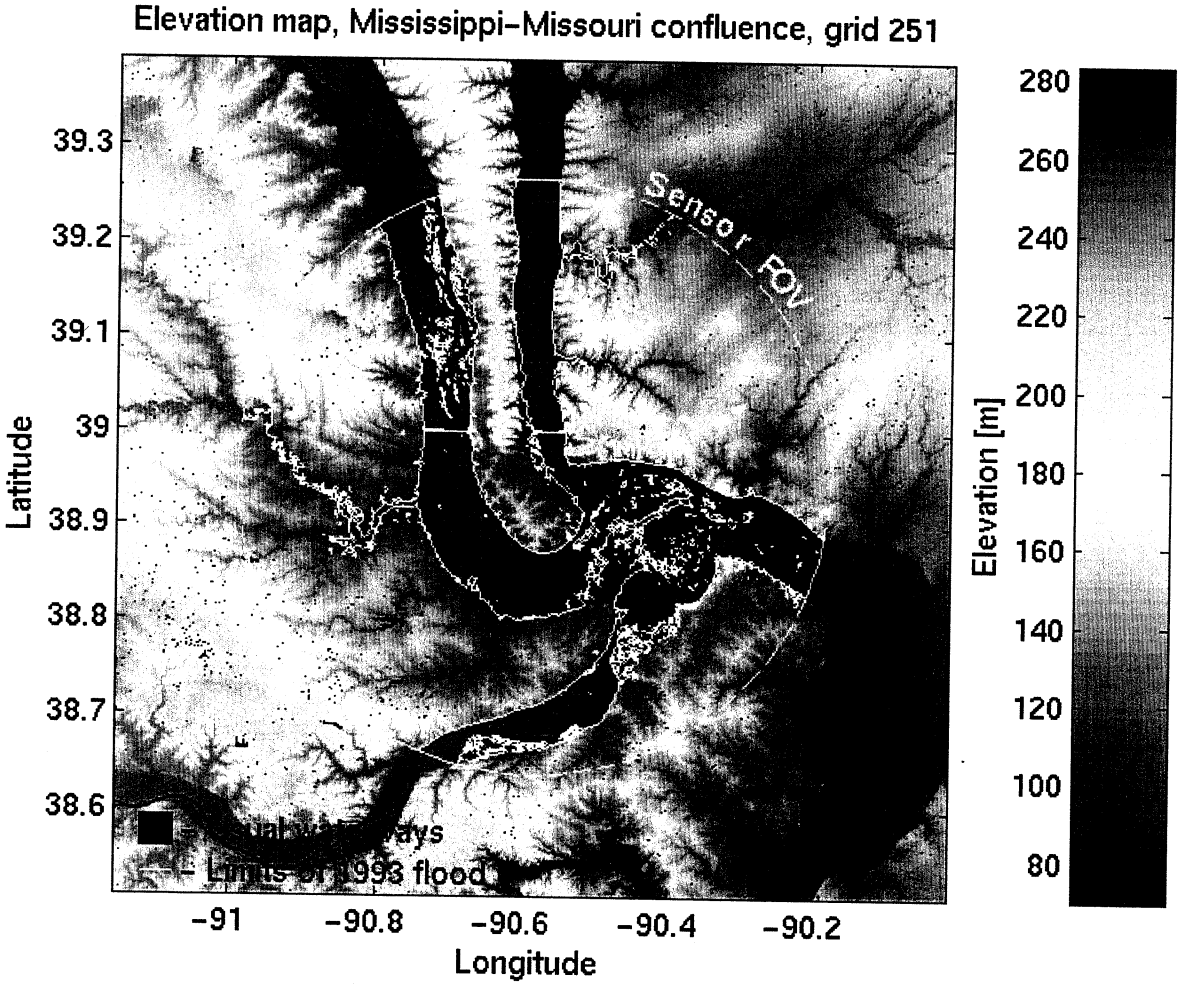

Figure I-1: Example elevation map made from SRTM DEMs. Four individual 1-degree square DEMs are merged and cropped relative to the brightness temperature FOV. Also plotted is the outline of an EASE-Gridded 70 km SSM/I sensor FOV and the 1993 flood limits from the SAST map.

REPORT DOCUMENTATION PAGE

Form Approved
OMB No. 0704-0188

1. AGENCY USE ONLY *(Leave blank)*	2. REPORT DATE	3. REPORT TYPE AND DATES COVERED
	9 Sept. 2002	Final report, 1 October 2000 - 30 September 2002

4. TITLE AND SUBTITLE
Final Report for SENH99-0000-0125 Real Time Monitoring of Flooding From Microwave Satellite Observations

5. FUNDING NUMBERS
C - NAS5-00189
G - SENH99-0000-0125

6. AUTHOR(S)
John F. Galantowicz

7. PERFORMING ORGANIZATION NAME(S) AND ADDRESS(ES)
Atmospheric and Environmental Research, Inc.
131 Hartwell Ave.
Lexington, MA 02421-3126

8. PERFORMING ORGANIZATION REPORT NUMBER
P870-FR-I-20020906

9. SPONSORING/MONITORING AGENCY NAME(S) AND ADDRESS(ES)
National Aeronautics and Space Administration
Goddard Space Flight Center
Code 219
Greenbelt, MD 20771

10. SPONSORING/MONITORING AGENCY REPORT NUMBER

11. SUPPLEMENTARY NOTES

12a. DISTRIBUTION AVAILABILITY STATEMENT
Publicly available

12b. DISTRIBUTION CODE

13. ABSTRACT *(Maximum 200 words)*

We have developed a new method for making high-resolution flood extent maps (e.g., at the 30-100 m scale of digital elevation models) in real-time from low-resolution (20-70 km) passive microwave observations. The method builds a "flood-potential" database from elevations and historic flood imagery and uses it to create a flood extent map consistent with the observed open water fraction. We present our method for transforming microwave sensor-scale open water fration estimates into high-resolution flood extent maps and describe 30-day flood map sequences generated during a retrospective study of the 1993 Great Midwest Flood. We discuss the method's potential improvement through as yet unimplemented algorithm enhancements and expected advancements in microwave radiometry (e.g., improved resolution and atmospheric correction).

14. SUBJECT TERMS
Flood extent, passive microwave remote sensing

15. NUMBER OF PAGES
30

16. PRICE CODE

17. SECURITY CLASSIFICATION OF REPORT	18. SECURITY CLASSIFICATION OF THIS PAGE	19. SECURITY CLASSIFICATION OF ABSTRACT	20. LIMITATION OF ABSTRACT
UNCLASSIFIED	UNCLASSIFIED	UNCLASSIFIED	UL